THE JOURNAL OF PHYSICAL CHEMISTRY C

Article

pubs.acs.org/JPCC

# High $CO_2$ Capture in Sodium Metasilicate ($Na_2SiO_3$) at Low Temperatures (30−60 °C) through the $CO_2$−$H_2O$ Chemisorption Process

Rafael Rodríguez-Mosqueda and Heriberto Pfeiffer*

Instituto de Investigaciones en Materiales, Universidad Nacional Autónoma de México, Circuito exterior s/n, Cd. Universitaria, Del. Coyoacán, México DF, CP 04510 Mexico

**ABSTRACT:** $Na_2SiO_3$ was synthesized by two different routes: solid-state reaction and combustion method. It was determined that $Na_2SiO_3$ sample prepared by the combustion method presented a surface area 3 times larger than the solid-state reaction sample. Different water vapor sorption experiments were performed using $N_2$ or $CO_2$ as carrier gases. If $N_2$ was used as carrier gas, it was evidenced that $Na_2SiO_3$ is able to trap water in two different ways: physically and chemically producing Na−OH and Si−OH species. Moreover, when $CO_2$ was used, $Na_2SiO_3$ continued trapping water, as in the previous case, but in this case $CO_2$ was trapped, forming $Na_2CO_3$ and $NaHCO_3$ phases. Additionally, as it could be expected, the surface area resulted to be a very important factor controlling the $CO_2$ capture efficiency. The $Na_2SiO_3$ sample prepared by the combustion method captured up to 8.5 mmol of $CO_2$ per gram of ceramic (efficiency of 52%), a considerably high $CO_2$ amount among different materials. Therefore, the presence of water vapor strongly favored the $CO_2$ chemisorption on $Na_2SiO_3$.

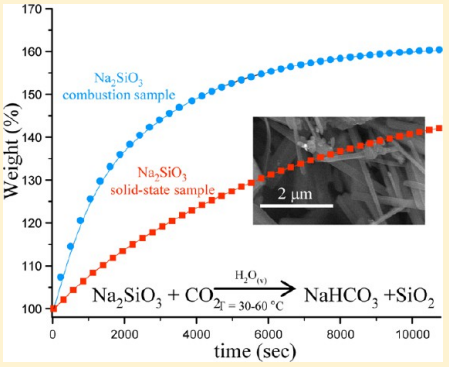


## INTRODUCTION

The carbon dioxide ($CO_2$) atmospheric concentration has increased significantly from 280 to 367 ppm in the past 250 years, increasing the so-called green-house effect and global warming.[1] Although the $CO_2$ increments include anthropogenic and natural emissions, human activity (combustion of fossil fuels, gas flaring, and cement production, among others) is mainly responsible for the equilibrium displacement.[2−6] Therefore, several strategies have been proposed to reduce or control, at least, the $CO_2$ emissions.[6,7]

Among the possible solutions, different materials have been studied as $CO_2$ captors at low (30−80 °C) or high ($T \geq 200$ °C) temperatures. However, the only commercially proven technology relies on aqueous $CO_2$ absorption on monoethanolamine (MEA).[8] In that sense, several materials that reversibly react or adsorb $CO_2$ at different temperatures have been proposed.[9−16] At low temperatures different activated carbons, hydrotalcites, zeolites, and other organic/inorganic cage structures have been tested as possible $CO_2$ captors, presenting some advantages and disadvantages.[9,10] Other groups of materials able to trap $CO_2$ at high and low temperatures are lithium or sodium zirconates, silicates, or aluminates,[9,11,14,15] where the $CO_2$ capture kinetics and efficiency depend on different factors such as the chemical composition, the structure, and different microstructural factors, among others.[17−44] For example, if the lithium ($Li_2ZrO_3$) and sodium ($Na_2ZrO_3$) metazirconate ceramics are compared, it has been observed that $Na_2ZrO_3$ possesses higher efficiencies and the $CO_2$ capture is produced in a wider temperature range than $Li_2ZrO_3$. The differences observed between these two ceramics have been related to structural features.[14] $Li_2ZrO_3$ has a dense monoclinic structure where lithium ion diffusion is hardly produced, while $Na_2ZrO_3$ possesses a layered monoclinic structure. In this case, sodium ions can diffuse much more efficiently, enhancing the $CO_2$ capture process. Additionally, it was recently published that $CO_2$ capture in $Na_2ZrO_3$ is importantly improved, at low temperatures (30−80 °C) under the water vapor presence,[19] producing sodium acid carbonate ($NaHCO_3$) instead of sodium carbonate ($Na_2CO_3$). It means that $Na_2ZrO_3$ can trap 1 or 2 mol of $CO_2$ per mole of ceramic, depending on the dry or humid conditions.

On the other hand, the $CO_2$ capture process in lithium ($Li_2SiO_3$) and sodium ($Na_2SiO_3$) metasilicates has not been deeply studied. In previous papers it has been shown that $Li_2SiO_3$ showed the ability to capture certain $CO_2$ under very specific conditions, where it was assumed that the synthesis route increased the reactivity of $Li_2SiO_3$ as a result of its small particle size and then its high surface area.[45,46] Conversely, $Na_2SiO_3$ had not been deeply analyzed. A few years ago, it was showed that $Na_2SiO_3$ was able to trap very low quantities of $CO_2$ at low temperatures under dry conditions.[47] Therefore, the aim of the present paper is to study the $CO_2$−$H_2O$ capture process on $Na_2SiO_3$, which may possess a high $CO_2$ capture capacity, if $NaHCO_3$ is produced.

**Received:** March 22, 2013
**Revised:** June 10, 2013
**Published:** June 10, 2013





dx.doi.org/10.1021/jp402850j | J. Phys. Chem. C 2013, 117, 13452−13461

## EXPERIMENTAL SECTION

The $Na_2SiO_3$ was synthesized using solid-state reaction and combustion methods. In the first case, the reagents employed were sodium carbonate ($Na_2CO_3$, Aldrich) and silicon oxide ($SiO_2$, Merck). The powders were mechanically mixed and then heated at 900 °C for 4 h. Finally, the $Na_2SiO_3$ product was pulverized. To obtain pure $Na_2SiO_3$, a 10 wt % excess of sodium was used during synthesis. Additionally, the same sample was prepared by the combustion method using sodium hydroxide (NaOH, Aldrich), $SiO_2$, and urea ($CO(NH_2)_2$, Aldrich). NaOH and urea were dissolved in the minimum water quantity, and then $SiO_2$ was dispersed in this solution, obtaining a viscous material, which was heated at 70 °C until dried. Finally, the powder was heat-treated at 500 °C for 5 min and then at 700 °C for 4 h in order to crystallize the material.

A diffractometer (Bruker AXS, D8 Advance) coupled to a copper anode X-ray tube was used to identify the phases obtained both during the synthesis and after the $CO_2$ capture process. The different phases and materials were identified using the Joint Committee Powder Diffraction Standards (JCPDS) files. In fact, the $Na_2SiO_3$ initial structure was confirmed by the 016-0818 JCPDS file (data not shown).The microstructural characteristics of the $Na_2SiO_3$ samples were determined via $N_2$ adsorption−desorption and scanning electron microscopy (SEM). For the $N_2$ adsorption−desorption experiments, the isotherms were acquired on a Bel-Japan Minisorp II at 77 K using a multipoint technique. The samples were degassed at room temperature for 24 h under vacuum prior to analysis. Then, the SEM experiments were performed on a JEOL JMS-7600F.

Dynamic and isothermal experiments were performed using a humidity-controlled thermobalance (TA Instruments, model Q5000SA) at different temperatures (30−60 °C) and relative humidities (RH). The experiments were performed using distilled water and two different carrier gases: nitrogen ($N_2$, Praxair grade 4.8) or carbon dioxide ($CO_2$, Praxair grade 3.0). The total gas flow rate used in all of the experiments was 60 mL/min, and the RH percentages were automatically controlled by the Q5000SA instrument. Dynamic water vapor sorption/desorption experiments were performed at different temperatures (between 30 and 60 °C), while varying the RH from 0 to 80% and then from 80 to 0% at a rate of 0.5%/min. Different isothermal experiments were performed at specific temperatures (30, 40, 50, and 60 °C) setting the RH at different values (20, 40, 60, and 80%) for each temperature, for 3 h using $CO_2$ as a carrier gas. Afterward, the products (~25 mg) were characterized to identify the hydration products. The samples were analyzed using X-ray diffraction (XRD), scanning electron microscopy (SEM), infrared spectroscopy (FTIR), and thermogravimetric analysis (TGA). The X-ray diffractometer and scanning electronic microscope used were already described above in the present section. For FTIR spectroscopy, samples were analyzed in a Nicolet 6700 spectrometer, using the ATR system. The TGA measurements were performed under a nitrogen atmosphere using a TA Instruments model Q500HR thermobalance at a heating rate of 5 °C/min. Finally, it should be mentioned that different thermodynamics calculations were performed using the HSC Chemistry 5.1 software.

## RESULTS AND DISCUSSION

The $N_2$ adsorption−desorption isotherm for the $Na_2SiO_3$ sample was acquired to determine its microstructural characteristics. The curve corresponds to a type II isotherm according to the IUPAC classification[48] (data not shown). The isotherm did not present hysteresis. This behavior corresponds to a nonporous, dense aggregate of particles. Additionally, the surface area of the sample was estimated to be 0.5 $m^2/g$ using the BET model. Figure 1 shows some of the morphological characteristics. The size of the $Na_2SiO_3$ agglomerates exceeded 30 $\mu$m (see the inset in Figure 1). A closer analysis indicated the presence of polyhedral particles, <1 $\mu$m in average. The two microstructural analyses ($N_2$ ads and SEM) are in good agreement with the synthesis method (solid-state reaction), which usually produces large and dense particles due to a sintering process.

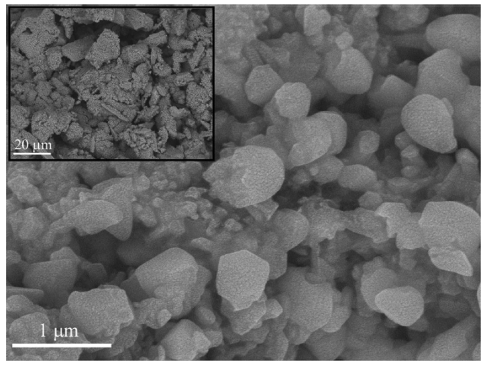


**Figure 1.** Backscattered electron images of the $Na_2SiO_3$ sample synthesized by solid-state reaction.

To further analyze and test this material, $CO_2$ sorption in presence of water vapor was studied. Based on theoretical thermodynamic data (HSC Chemistry 5.1 software), the reaction between $Na_2SiO_3$ and $CO_2$ in dry conditions can take place at temperatures lower than 330 °C (Figure 2).

$$Na_2SiO_3 + CO_{2(g)} \rightarrow Na_2CO_3 + SiO_2 \quad (1)$$

In fact, Rodríguez and Pfeiffer[47] reported that $CO_2$ capture on $Na_2SiO_3$ occurs in spite of its low reactivity and kinetic factors. On the other hand, some researchers have reported water vapor addition affects the $CO_2$ capture of lithium and sodium ceramics.[19,30,46,49] They have observed that water addition enhances kinetic properties even at low temperatures. Thus, with these antecedents and taking into consideration the theoretical thermodynamic data (Figure 2A) calculated according to the reaction 2, the $CO_2$ capture process in $Na_2SiO_3$ in presence of water vapor was carried out.

$$Na_2SiO_3 + 2CO_{2(g)} + H_2O_{(v)} \rightarrow 2NaHCO_3 + SiO_2 \quad (2)$$

If the Gibbs free energy ($\Delta G$) values of reactions 1 and 2 are compared, the presence of water vapor clearly induces the $NaHCO_3$ formation (reaction 2) over the $Na_2CO_3$ formation (reaction 1) at $T \leq 130$ °C. Additionally, something else has to be pointed out—the quantity of $CO_2$ that can be trapped by $Na_2SiO_3$, in the presence of water, is double that captured in reaction 1. Hence, in this case, $Na_2SiO_3$ has a maximum theoretical $CO_2$ chemisorption capacity of 16.39 mmol/g. Additionally, it is known that the equilibrium constant ($K$) is related to the $\Delta G$ through the equation $K = \exp(-\Delta G_0/RT)$


dx.doi.org/10.1021/jp402850j | J. Phys. Chem. C 2013, 117, 13452−13461

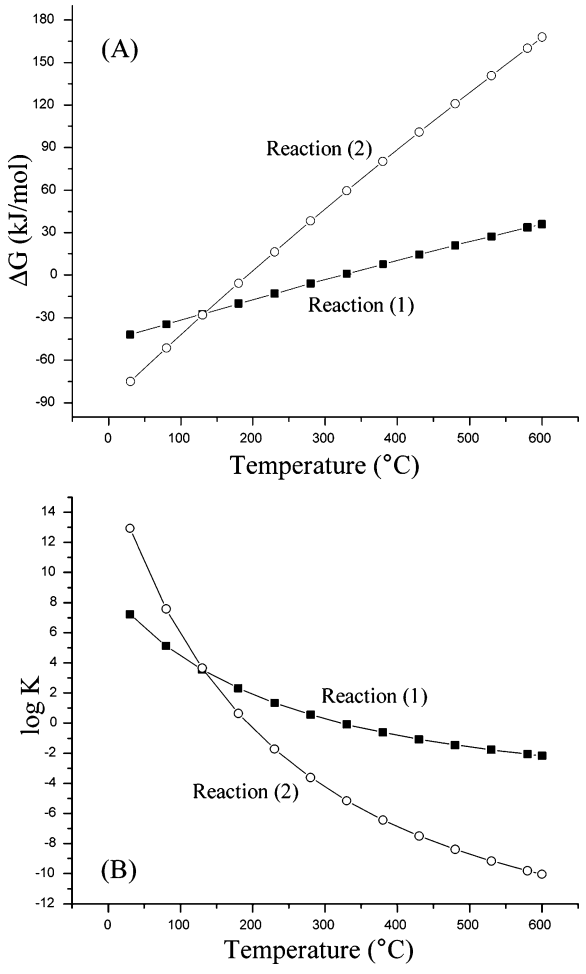


**Figure 2.** Gibbs free energy (A) and equilibrium constant (B) changes as a function of the temperature for the $CO_2$ chemisorption on $Na_2SiO_3$ in dry (reaction 1) and humid (reaction 2) conditions.

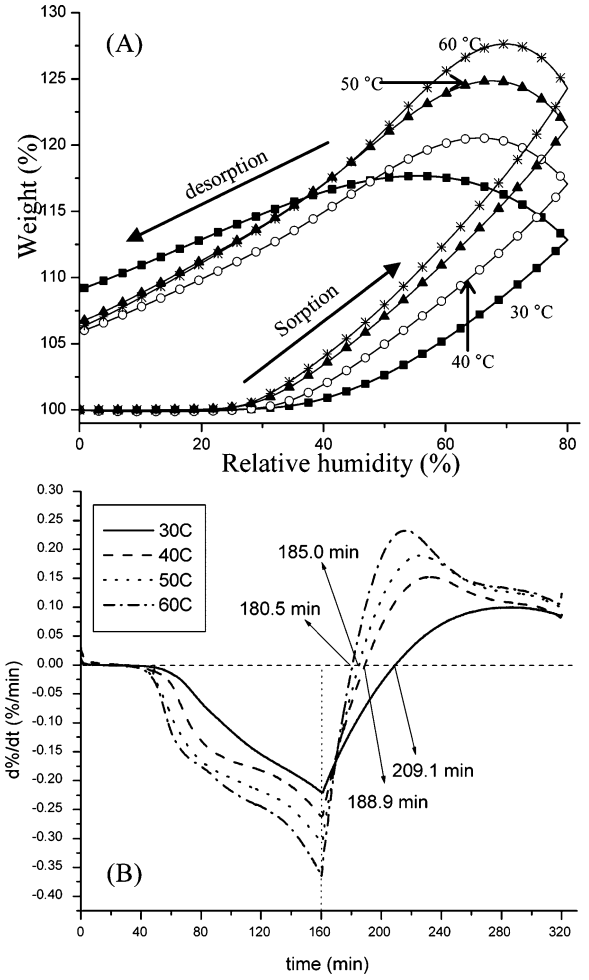


**Figure 3.** Water vapor isotherms of the $Na_2SiO_3$ sample (A), generated at temperatures between 30 and 60 °C, using $N_2$ as carrier gas. The derivative thermograms, as a function of time, of the same water vapor isotherms (B). Each curve represents the experimental data, and the symbols were used to differentiate them.

(see Figure 2B). Finally, it must be taken into account that the reaction 2 $K$ value is 6 orders of magnitude larger than that of reaction 1 at $T \leq 50$ °C. Therefore, the presence of water vapor importantly increases the displacement of the equilibrium to the product formation.

First, $Na_2SiO_3$ was exposed to water vapor at different temperatures (30−60 °C) using $N_2$ as carrier gas. These experiments were performed seeking for any possible reaction between sodium metasilicate and water vapor. Figure 3 shows water vapor sorption/desorption isotherms. It is clearly evident that all of the sorption isotherms corresponded to type III according to the IUPAC classification.[48] Additionally, the water sorption varied as a function of the temperature, and it was not completed or limited to the increasing relative humidity section ramp (0−80% RH) because during some part of the decreasing RH section ramp (80−0% RH), the samples continued gaining weight. The continuous weight increment observed at the beginning of the RH decrease ramp is an indicative that the water vapor sorption continued at these temperatures and RH conditions because the equilibrium has not been reached in these dynamic experiments. When the $Na_2SiO_3$ sample was treated at 30 °C, the maximum water sorption was equal to 17.7 wt %, but this quantity increased as a function of the temperature to 27.6 wt % at 60 °C. Additionally, the sorption process began at lower RH when temperature was increased. At 30 °C, the weight increased at around 38% of RH, while the sorption process began with 24.7% of RH at 60 °C. Afterward, the final water desorption was proportional to the temperature, which may be attributed to water evaporation; while the final water trapped was 9 wt % at 30 °C (0% of RH), the water trapped decreased to ∼6.3 wt % at all the other temperatures. Although the final water trapped did not changed significantly, the evaporation rate did. Figure 3B shows the DTG curves of the weight change as a function of time. From the second part of these curves (after the 160 min vertical line) it is clearly evident that evaporation process (seen as a change in the sign of the derivative) began at shorter times if temperature was increased. While at 30 °C the evaporation began after 209.1 min, this time was decreased to 180.5 min at 60 °C. It is seen from the magnitude of the maximum derivative values that the evaporation rate was larger as a function of temperature. In other alkaline and earth alkaline ceramics, it has been shown that the weight gained at the end of similar isothermal experiments can be attributed to $H_2O$ that is physisorbed and/or chemically (formation of Na−OH and/or Si−OH species) trapped.[19,30,46,49]

Figure 4 shows the $Na_2SiO_3$ water sorption−desorption curves using $CO_2$ as carrier gas. Although the sorption curves


dx.doi.org/10.1021/jp402850j | J. Phys. Chem. C 2013, 117, 13452−13461

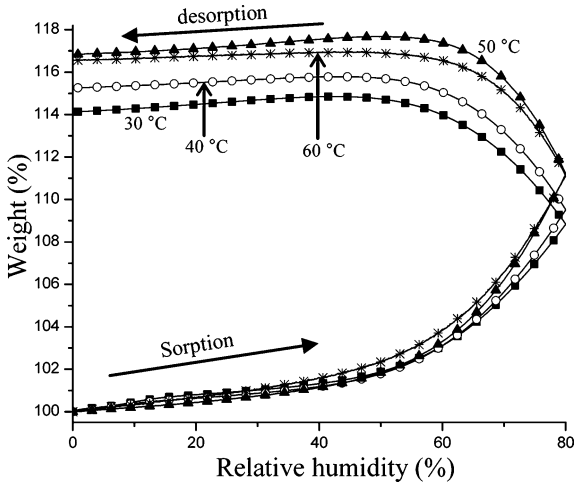


**Figure 4.** Water vapor isotherms of the $Na_2SiO_3$ sample, generated at temperatures between 30 and 60 °C, using $CO_2$ as carrier gas. Each curve represents the experimental data, and the symbols were used to differentiate them.

were type III, as in the $N_2$ case, the water desorption process and the final weight increments were noticeably different. During the sorption process, the weight increments increased as a function of the temperature. The final weights observed after the desorption process increased between 30 and 50 °C, from 14.1 to 16.9 wt %. However, at 60 °C, the weight increment decreased slightly to 16.6 wt %. In any case the final weight increments were always higher than those observed when a $N_2$−$H_2O$ flow was used. Therefore, the $CO_2$−$H_2O$ flow must produce a different reaction process—the hydration, hydroxylation, and carbonation of $Na_2SiO_3$—and the hydration may have been reduced at the highest temperature (60 °C) because of water evaporation.

To analyze the $Na_2SiO_3$−$CO_2$−$H_2O$ products, some of the isothermal products were analyzed using FTIR and XRD. Figure 5 shows the FTIR spectra of the $Na_2SiO_3$ initial sample and $Na_2SiO_3$ samples isothermically treated at 40, 50, and 60 °C into a $CO_2$−$H_2O$ flow. The $Na_2SiO_3$ initial sample presented different metal−oxygen vibration bands (Na−O and Si−O) between 400 and 1000 $cm^{-1}$ associated with this phase. Additionally, it should be mentioned that there were not identified any hydroxyl (3000 and 3500 $cm^{-1}$)[50] and/or carbonate (between 850 and 1410 $cm^{-1}$)[50]) species. On the contrary, the $Na_2SiO_3$ samples treated into a $CO_2$−$H_2O$ flow at different temperatures presented similar FTIR spectra among them, where the following vibration bands were detected. Although metal−oxygen vibration bands were still present, as it could be expected, a wide O−H vibration band was detected between 3000 and 3500 $cm^{-1}$, corresponding to adsorbed water and/or hydroxyl species produced at the $Na_2SiO_3$ surface. In fact, this band was more evident in the sample treated at the lowest temperature (40 °C), as the evaporation process is less produced. Moreover, two different phases were evidenced by new vibration bands. While the vibration bands detected at 702, 877, and 1410 $cm^{-1}$ correspond to $Na_2CO_3$,[51] the vibration bands located at 835, 1000, 1035, 1295, 1620, 1660, and 1906 $cm^{-1}$ fit to the $NaHCO_3$ FTIR spectrum.[51] Some of these peaks seem to decrease as a function of temperature, although the final weight increments observed in the Figure 4 increased. Figure 5B shows two characteristic vibration bands of $Na_2CO_3$ (877 $cm^{-1}$) and $NaHCO_3$ (835 $cm^{-1}$), where the $Na_2CO_3$/

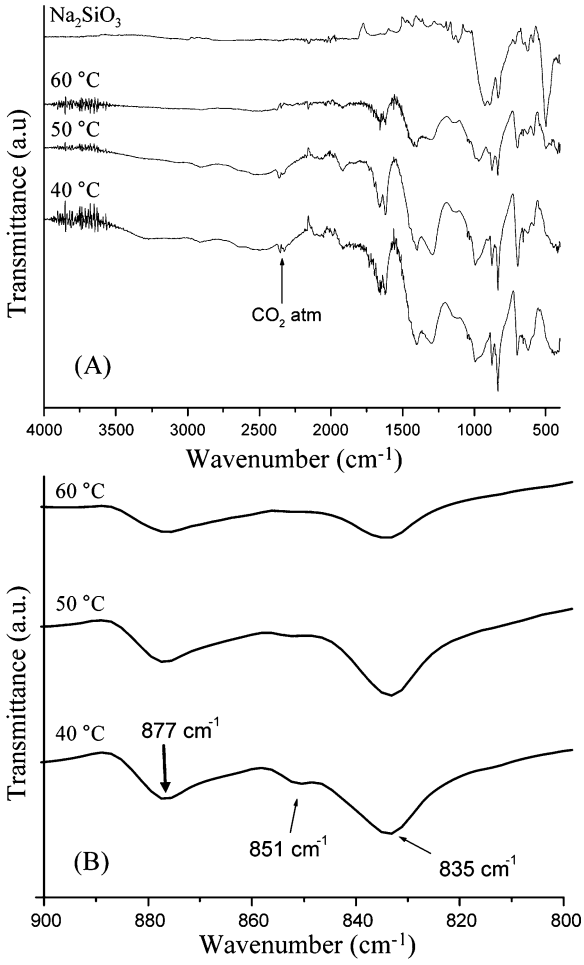


**Figure 5.** ATR-FTIR spectra of the $Na_2SiO_3$ initial sample and $Na_2SiO_3$ samples isothermically treated at 40, 50, and 60 °C into a $CO_2$−$H_2O$ flow (A). A specific zoom showing the $Na_2CO_3$ and $NaHCO_3$ vibration bands between 800 and 900 $cm^{-1}$ (B).

$NaHCO_3$ intensity bands ratio slightly increases with temperature. It must be mentioned that the vibration band located at 831 $cm^{-1}$ corresponds to a $CO_3^{2-}$ vibration mode of the $Na_2CO_3$·$NaHCO_3$·$2H_2O$ system.[52] These results confirm the $NaHCO_3$ formation but as well the presence of $Na_2CO_3$. In fact, temperature seems to inhibit the $NaHCO_3$ formation. In addition, the carbonate phases were confirmed by XRD. Figure 6 shows the XRD pattern of the $Na_2SiO_3$ sample previously treated at 60 °C into the $CO_2$−$H_2O$ flow. As it can be seen, the main peaks correspond to $Na_2SiO_3$, but there were other small peaks that can be attributed to $Na_2CO_3$ and/or $NaHCO_3$, as the diffraction peaks of these two carbonates are very close. Crystalline $SiO_2$ was not detected in the XRD pattern, according to reactions 1 and 2. Thus, it may be produced as an amorphous phase. In any case, the formation of these diffraction peaks confirmed the FT-IR analysis and consequently the $CO_2$ chemical reaction with $Na_2SiO_3$ at this temperature range.

It has been described in the literature[47] that $Na_2SiO_3$ chemisorbs small amounts of $CO_2$ (≤1 wt %) at dry conditions (see reaction 1). Nevertheless, the water vapor allowed the $CO_2$ chemisorption to occur in much higher quantities. Thus, water molecules should react with $Na_2SiO_3$ superficially, producing Na−OH and Si−OH species. Then, the activated surface must be more reactive to $CO_2$. Therefore, $Na_2SiO_3$ may have reacted


dx.doi.org/10.1021/jp402850j | J. Phys. Chem. C 2013, 117, 13452−13461

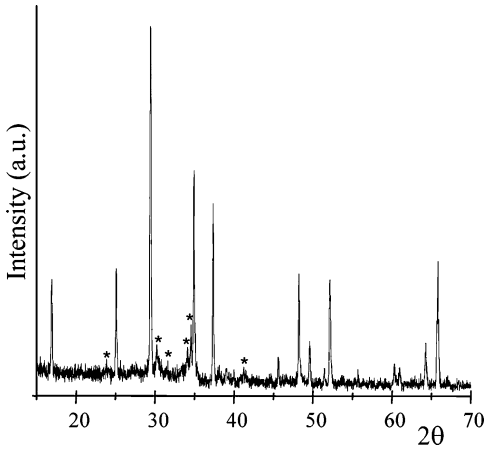


**Figure 6.** XRD pattern of the $Na_2SiO_3$ sample isothermally treated at 60 °C into a $CO_2$−$H_2O$ flow. The peaks labeled with an asterisk can correspond to the $Na_2CO_3$ (01-086-0291 file) and/or $NaHCO_3$ (96-901-1049 file).

with $CO_2$ because of a superficial hydroxylation, according to the following reactions:

$$Na_2SiO_3 \xrightarrow{H_2O} Na_2SiO_{3(\text{superficially activated})} \quad (3)$$

$$Na_2SiO_{3(\text{superficially activated})} + 2CO_2 \rightarrow 2NaHCO_3 + SiO_2 \quad (4)$$

In fact, reaction 4 may be divided in the following two step-reactions, the $Na_2CO_3$ formation and the subsequent $NaHCO_3$ production:

$$Na_2SiO_{3(\text{superficially activated})} + CO_2 \rightarrow Na_2CO_3 + SiO_2 \quad (5)$$

$$Na_2CO_3 + CO_2 + H_2O \rightarrow 2NaHCO_3 \quad (6)$$

Additionally, some microstructure characteristics were evaluated by SEM in the $Na_2SiO_3$ sample after the $CO_2$−$H_2O$ process. As it can be seen, in Figure 7, the morphology of

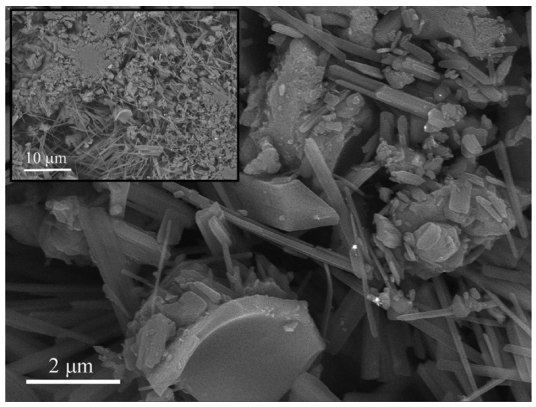


**Figure 7.** Backscattered electron images of the $Na_2SiO_3$ sample isothermically treated at 50 °C into a $CO_2$−$H_2O$ flow.

the sample changed significantly, in comparison to the initial $Na_2SiO_3$ (see Figure 1). New filament-like structures appeared in the morphology, which must be associated with the $Na_2CO_3$ and $NaHCO_3$ formation. These filaments were as large as 7.5 μm, with different thickness (0.2−0.3 μm). The surface of these particles was considerably smooth. Therefore, the formation of these carbonate filaments does not produce a rigid external shell over the $Na_2SiO_3$ particles. This particle growth must allow a further $CO_2$ chemisorption.

To further understand the influence of RH in the $Na_2SiO_3$−$CO_2$−$H_2O$ system, different kinetic experiments are presented in Figure 8, which correspond to the experiments performed at different temperatures (30, 40, 50, and 60 °C) and RH (20, 40, 60, and 80%). For each temperature, the weight increment rates increased as a function of the RH, as it could be expected. For example, at 50 °C (Figure 8C) the samples treated with 20 and 40% of RH only increased their weights in 2.0 and 4.0 wt % after 3 h, respectively. However, when the RH was increased to 60 and 80%, the final weight increments were equal to 11.5 and 42 wt %, respectively. However, a more interesting behavior can be observed if the isotherms are analyzed as a function of the temperature. Figure 9 shows the isotherms treated with 80% of RH at different temperatures. In this case, the final weight increments were 30.6% (30 °C), 41.3% (40 °C), 42.1% (50 °C), and 27.0% (60 °C). The final weight increment at 60 °C decreased, and it may be associated with the $NaHCO_3$ inhibition from $Na_2CO_3$, evidenced previously, which reduces the weight increments importantly.

To quantify the $CO_2$ capture through the $NaHCO_3$ and $Na_2CO_3$ formation under the different thermal and RH conditions, all of the isothermal products were characterized using TGA. As example, Figure 10 shows the TGA and DTG curves of $Na_2SiO_3$ that was isothermally treated at 50 °C with different RHs. These thermograms show two different temperature decomposition ranges. Initially, between room temperature and 200 °C, the samples lost different quantities of weight, which could be attributed to dehydration and $NaHCO_3$ decomposition processes. In the DTG curves, at temperatures lower than 78 °C, there is one peak, corresponding to a drying process. The intensity of this peak increased as a function of the RH, as it could be expected. Then, between 78 and 200 °C the DTG presented several peaks associated with the $NaHCO_3$ decomposition process.[52] The $NaHCO_3$ decomposition process has been described, producing $Na_2CO_3$ and two gas species, $H_2O$ and $CO_2$, accordingly to the following reaction[53]

$$2NaHCO_3 \rightarrow Na_2CO_3 + CO_{2(g)} + H_2O_{(v)} \quad (7)$$

The presence of other DTG peaks may be associated with the thermal decomposition of other mixed hydrated-carbonate phases such as $Na_2CO_3{\cdot}3NaHCO_3$, $Na_2CO_3{\cdot}NaHCO_3{\cdot}2H_2O$, and $Na_2CO_3{\cdot}H_2O$, as was already evidenced by FTIR. However, it was assumed that the only decomposition present in this temperature range was the one of the $NaHCO_3$ single salt. Therefore, the weight lost observed in this temperature range (78 °C ≤ $T$ ≤ 200 °C) can be associated with the $CO_2$ and $H_2O$ liberation, where each compound theoretically contributes in 70.9 and 29.1% of the corresponding total weight lost observed (see eq 7). The dehydroxylation process was attributed to the continuous weight lost observed in the TG curves between 200 and 400 °C. In fact, the samples treated at lower RH almost not presented this process. Finally, the weight lost observed at $T$ ≥ 600 °C was attributed to the $Na_2CO_3$ decomposition process. All of the samples presented a decarbonation process (reaction 8), which appeared to increase as a function of the RH.

$$Na_2CO_3 + SiO_2 \rightarrow Na_2SiO_3 + CO_{2(g)} \quad (8)$$

Therefore, to quantify the amounts of $CO_2$ trapped (as $NaHCO_3$ or $Na_2CO_3$) by $Na_2SiO_3$, all of the weight variations


dx.doi.org/10.1021/jp402850j | J. Phys. Chem. C 2013, 117, 13452−13461

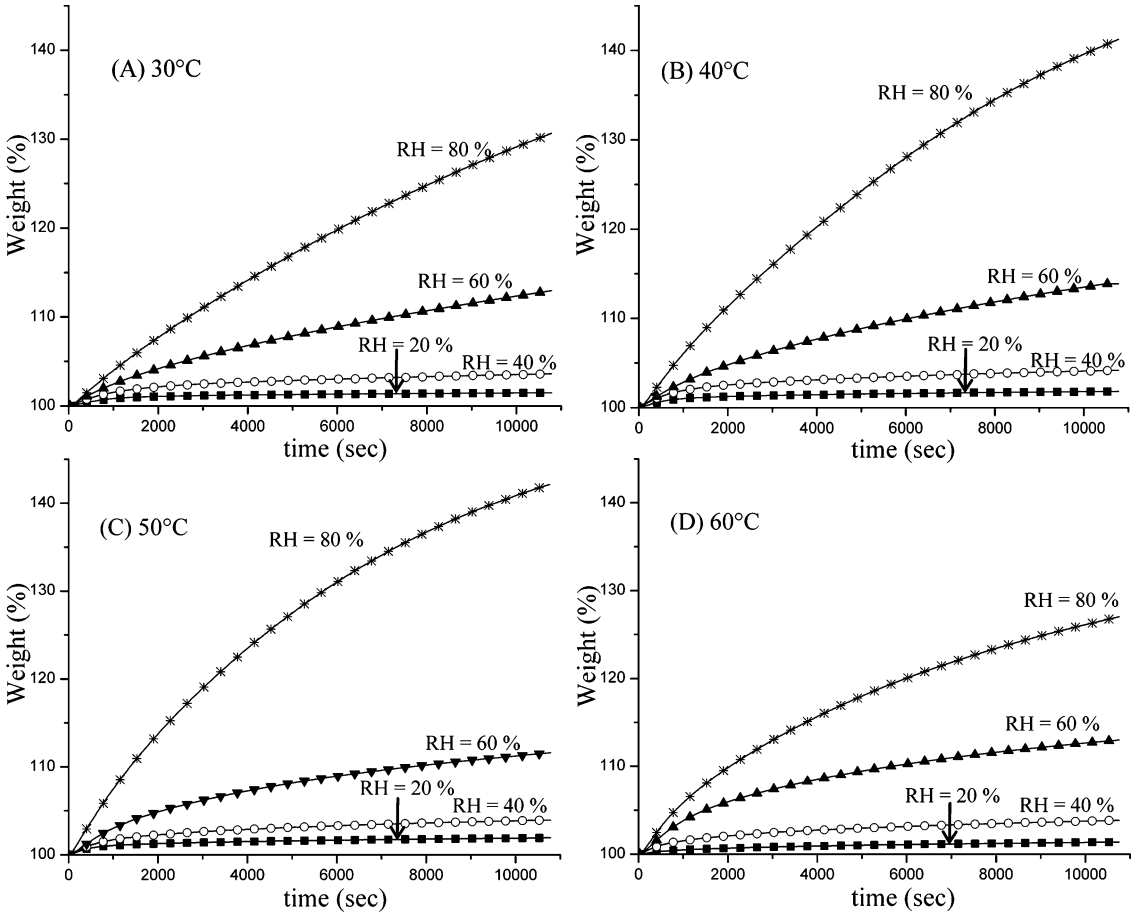


**Figure 8.** Kinetic isotherms performed at different temperatures (30, 40, 50, and 60 °C) and RH (20, 40, 60, and 80%) with a $CO_2$ flow of 60 mL/min. Each curve represents the experimental data, and the symbols were used to differentiate them.

determined from the TGA experiments are plotted in Figure 11. It must be mentioned that the $CO_2$ quantities reported in these plots correspond to the total $CO_2$ desorbed by the $NaHCO_3$ and $Na_2CO_3$ decomposition processes (reactions 7 and 8). It is clearly evident that when the RH was increased from 20 to 80%, the total amount of $CO_2$ chemisorbed increased, independently of the temperature, although the $CO_2$ chemisorbed decreased at 60 °C for 80% RH, in comparison to the other temperatures. As it can be seen, the maximum weight increment (16.5 wt %) was obtained under the following conditions; 40 °C and 80% of RH, which corresponds to a 28.4% efficiency, assuming reaction 4 as $CO_2$ chemisorption model. This efficiency values are equal to 4.66 mmol of $CO_2$ per gram of $Na_2SiO_3$ (mmol/g), where the maximum theoretical value is 16.39 mmol/g. All these results clearly show that $CO_2$ chemisorption in $Na_2SiO_3$ is importantly improved by the presence of water vapor in this temperature range, in comparison to the dry conditions. Additionally, the $Na_2SiO_3$ sample treated in the presence of water vapor appears to be capable of chemically trapping as much $CO_2$ as many other materials at moderate temperatures (30−80 °C), including activated carbons, zeolites, hydrotalcites, and amines, where the maximum $CO_2$ chemisorption values are around 4−6 mmol/g.[9]

As it has been shown in previous papers,[21,40,44,46] the $CO_2$ capture efficiency can be modified by the initial surface area. Therefore, the $Na_2SiO_3$ was synthesized by the combustion method in order to obtain a larger surface area, which may enhance the $CO_2$ capture. After the corresponding $Na_2SiO_3$ structural (XRD) and microstructural ($N_2$ adsorption and SEM) characterizations (data not shown), it was confirmed the $Na_2SiO_3$ synthesis and the variation of microstructural properties as the BET surface area increased to 1.6 $m^2/g$, in comparison to the previous solid-state sample (0.5 $m^2/g$). It means 3 times more surface area. Figure 12 shows the SEM image of this sample. It can be seen that $Na_2SiO_3$ particles has morphological variations in comparison to the solid-state sample. In this case, the particles seem to be sintered forming irregular particles of around 10 $\mu$m. However, these particles presented a corrugated surface, which may be responsible of the larger surface area determined by $N_2$ adsorption.

Again, the $CO_2$−$H_2O$ capture behavior of the $Na_2SiO_3$ synthesized by the combustion method was tested (Figure 13). In this figure, it was added the isotherm performed at 50 °C with the $Na_2SiO_3$ solid-state sample, for comparison purposes. Again, all the sorption curves were type III, as in the solid-state sample. Nevertheless, the initial sorption processes and final weight increments were considerably higher. In addition, the final weight increments (between 41.5 and 47.0 wt %) observed in the combustion sample were more than twice larger than those observed in the solid-state sample.

The final weight increments observed after the desorption process increased between 30 and 40 °C from 41.5 to 47.0 wt %, but at 50 and 60 °C the weight increments decreased to 44.0 and 41.7 wt %, respectively. In the solid-state case, only at 60 °C it was observed the final sorption decrement and it was


dx.doi.org/10.1021/jp402850j | J. Phys. Chem. C 2013, 117, 13452−13461

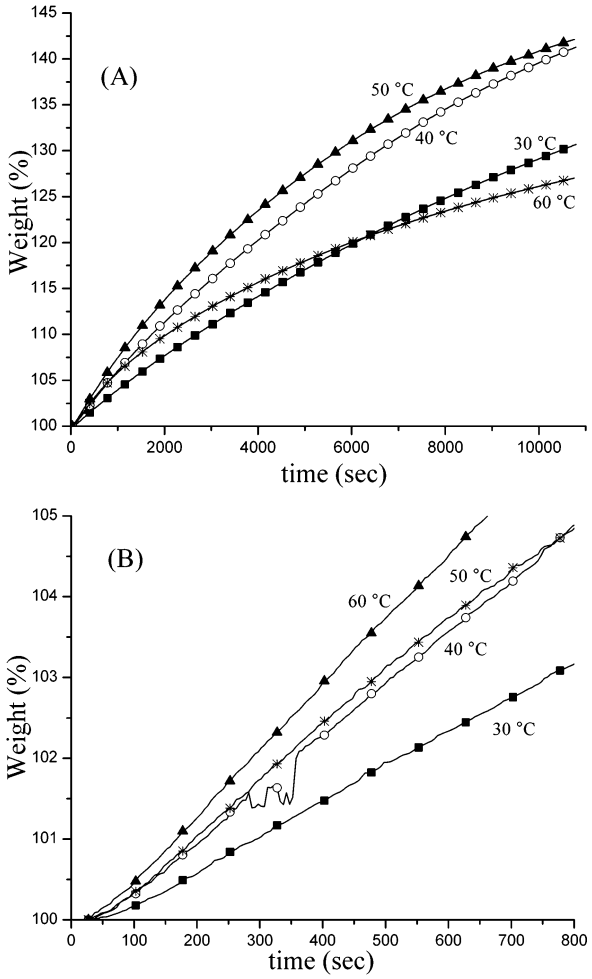


**Figure 9.** Comparison of the different kinetic isotherms performed between 30 and 60 °C with 80% of RH (A). First 800 s of the isotherms performed between 30 and 60 °C with 80% of RH (B). Each curve represents the experimental data, and the symbols were used to differentiate them.

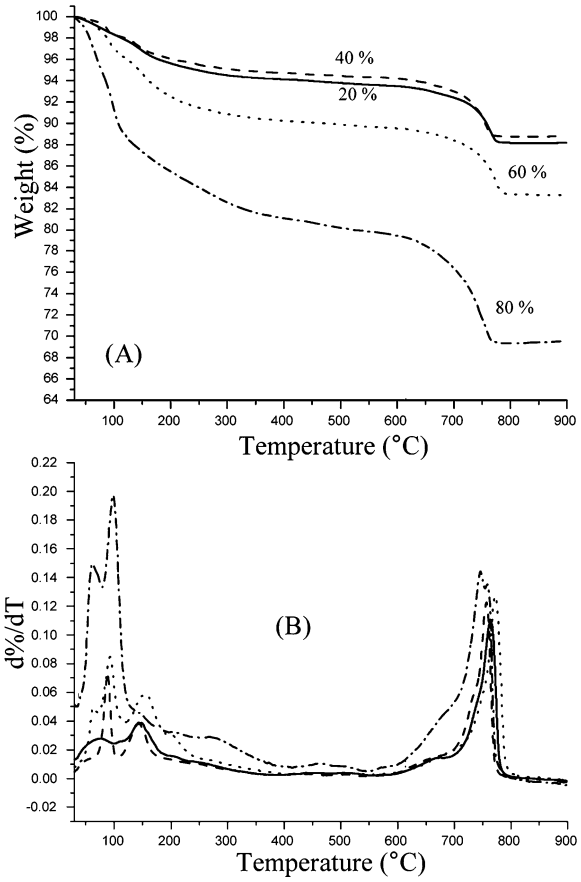


**Figure 10.** TG (A) and DTG (B) curves of $Na_2SiO_3$ samples isothermally treated at 50 °C and different RH (20−80%).

attributed to the water evaporation. Therefore, in this case, as the weight increments were higher, due to the surface area, the water adsorption may be larger as well, producing an important evaporation since 50 °C. In any case, if the water adsorption was higher, the $CO_2$ capture, as $NaHCO_3$ and $Na_2CO_3$, must be higher as well.

In order to prove it, different and specific isothermal experiments were performed to quantify the total $CO_2$ chemisorbed by the $Na_2SiO_3$ combustion sample. Figure 14A shows four isotherms performed at 50 °C at different RH. As it could be expected, the isotherms increased their weights as a function of the RH, reaching final weight increments of 13, 24.9, 40.2, and 60.3 wt %, for RH of 20, 40, 60, and 80%, respectively. If these results are compared to those obtained with the $Na_2SiO_3$ solid-state sample (Figure 8C), it can be seen a very important increment of $CO_2$−$H_2O$ sorbed, which may be attributed to the surface area. For example, in the solid-state sample the isotherms performed between 20 and 60% of RH did not increase their weights (wt < 13%) more than the combustion sample (wt = 13%) with 20% of RH. Specifically, Figure 14B shows a comparison between $Na_2SiO_3$ samples prepared by solid-state and combustion methods isothermically treated at 50 °C and 80% of RH and the corresponding TG decomposition experiments of the final corresponding products. From the isothermal experiments, it is clearly evident that the $Na_2SiO_3$ sample prepared by the combustion method gained faster and more weight than the solid-state sample. In fact, after 3 h the combustion sample gained ∼20% more weight than the solid-state sample. Finally, although the TG decomposition thermograms showed similar trends, the weight lost observed in the different steps were larger in the combustion samples (Figure 14C). The $NaHCO_3$ decomposition process associated with the second weight lost showed decrements of 8.78 and 27.19 wt % for the solid-state and combustion samples, respectively. Then, the weight lost associated with the $Na_2CO_3$ decomposition ($T \geq 600$ °C) presented differences as a function of the $Na_2SiO_3$ sample as well. In the solid-state sample the weight lost was 10.35 wt % and the combustion sample presented a weight loss of 18.32 wt %; however, in this sample the $Na_2CO_3$ decomposition did not finished, as the wt % continued decreasing above 900 °C. Moreover, in the combustion sample, it was evident a third weight loss at around 450 °C, associated with the dehydroxylation process. As this sample has a larger surface area, all the sorption phenomena are extrapolated and consequently more evident. Results obtained from the $Na_2SiO_3$ combustion sample showed an important $CO_2$ capture increment. This sample was able to increase the $CO_2$ capture efficiency to 52%, corresponding to a final $CO_2$ capture of 8.5 mmol/g, almost twice the $CO_2$ captured by the solid-state sample (4.6 mmol/g). Therefore, the $Na_2SiO_3$ prepared by the combustion method is able to trap more $CO_2$ than other


dx.doi.org/10.1021/jp402850j | J. Phys. Chem. C 2013, 117, 13452−13461

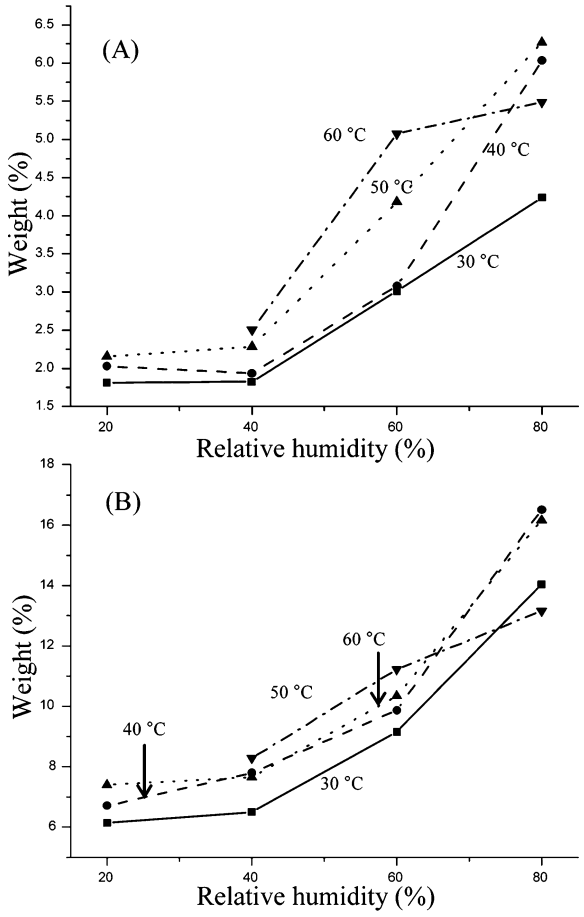


**Figure 11.** Quantification of the $CO_2$ desorbed during the TG analyses from $NaHCO_3$ (A) and $Na_2CO_3$ (B) by $Na_2SiO_3$, varying temperature and RH.

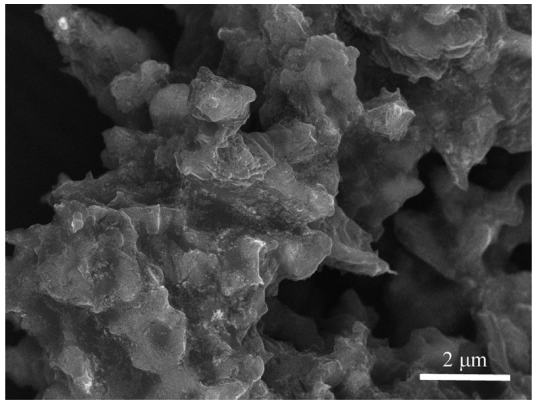


**Figure 12.** Backscattered electron images of the $Na_2SiO_3$ sample synthesized by the combustion method.

materials such as zeolites, hydrotalcites, and activated carbons.[9] Thus, $Na_2SiO_3$ must be considered as a possible option for the $CO_2$ capture process at moderated or environmental temperatures.

Summarizing, $Na_2SiO_3$ is able to trap, chemically, high $CO_2$ quantities in the presence of water vapor. The $CO_2$ trapped produced $Na_2CO_3$ and $NaHCO_3$ as products. The formation of these carbonates was determined by the temperature, but mainly as a function of the relative humidity. Finally, the quantities of $CO_2$ trapped by the $Na_2SiO_3$ are higher in

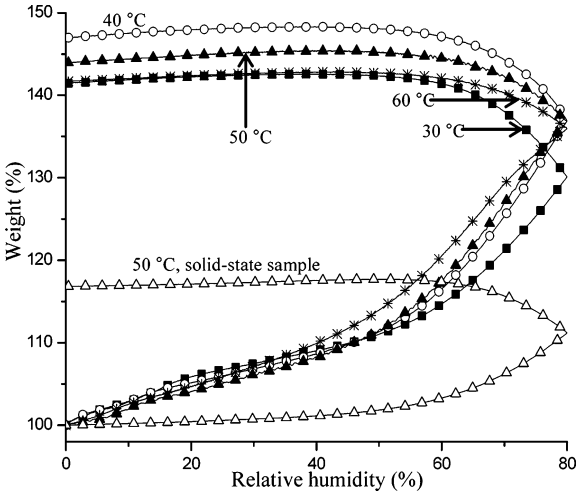


**Figure 13.** Water vapor isotherms of the $Na_2SiO_3$ sample prepared by combustion method, generated at temperatures between 30 and 60 °C, using $CO_2$ as carrier gas. The 50 °C isotherm of the $Na_2SiO_3$ sample prepared by solid-state reaction was added for comparison purposes. Each curve represents the experimental data, and the symbols were used to differentiate them.

comparison to other materials. Therefore, more and deeper analyses have to be performed on the $Na_2SiO_3$–$CO_2$–$H_2O$ system, as in this temperature range, most of the materials used trap $CO_2$ physically (zeolites, activated carbons, etc.). In the present case, as the $CO_2$ is chemically trapped, $CO_2$ desorption must be performed chemically or at high temperatures, which may be an interesting industrial issue. However, in the present case, the $CO_2$ chemisorption is selective and it is not necessarily limited to the surface, which may be an important advantage over the $CO_2$ physisorbent materials.

## CONCLUSIONS

The $CO_2$–$H_2O$ sorption process on $Na_2SiO_3$, with different microstructural properties, was evaluated at low temperatures (30–60 °C). $Na_2SiO_3$ samples were prepared by solid-state and combustion methods in order to obtain different textural properties. The surface areas obtained were 0.5 and 1.6 $m^2/g$ for the solid-state and combustion methods, respectively.

Initial results, using $N_2$ as carrier gas, showed that $Na_2SiO_3$ traps water physically and chemically, where the water vapor adsorption and/or absorption depended on temperature and relative humidity. When $CO_2$ was used as carrier gas, important changes appeared in the results. Although $Na_2SiO_3$ continued trapping water, by the same mechanisms, $CO_2$ was chemically trapped as well, producing $Na_2CO_3$, $NaHCO_3$, and $SiO_2$. In fact, different isothermal analyses and the characterization of the isothermal products showed that the formation of $NaHCO_3$ was determined by the temperature, but mainly as a function of the relative humidity. It means that under the thermal humidity conditions, $Na_2SiO_3$ would be able to absorb up to 16.39 mmol of $CO_2$ per gram of ceramic, which is 2 times more $CO_2$ than the quantity absorbed under dry conditions.

Additionally, it was probed that the $Na_2SiO_3$ sample prepared by the combustion method (larger surface area) showed an important $CO_2$ capture increment, in comparison to the $Na_2SiO_3$ solid-state reaction sample. The combustion sample increased its $CO_2$ capture efficiency to 52% (8.5 mmol/g), almost twice the $CO_2$ captured by the solid-state sample (4.6 mmol/g). The $CO_2$ capture efficiency differences in these


dx.doi.org/10.1021/jp402850j | J. Phys. Chem. C 2013, 117, 13452–13461

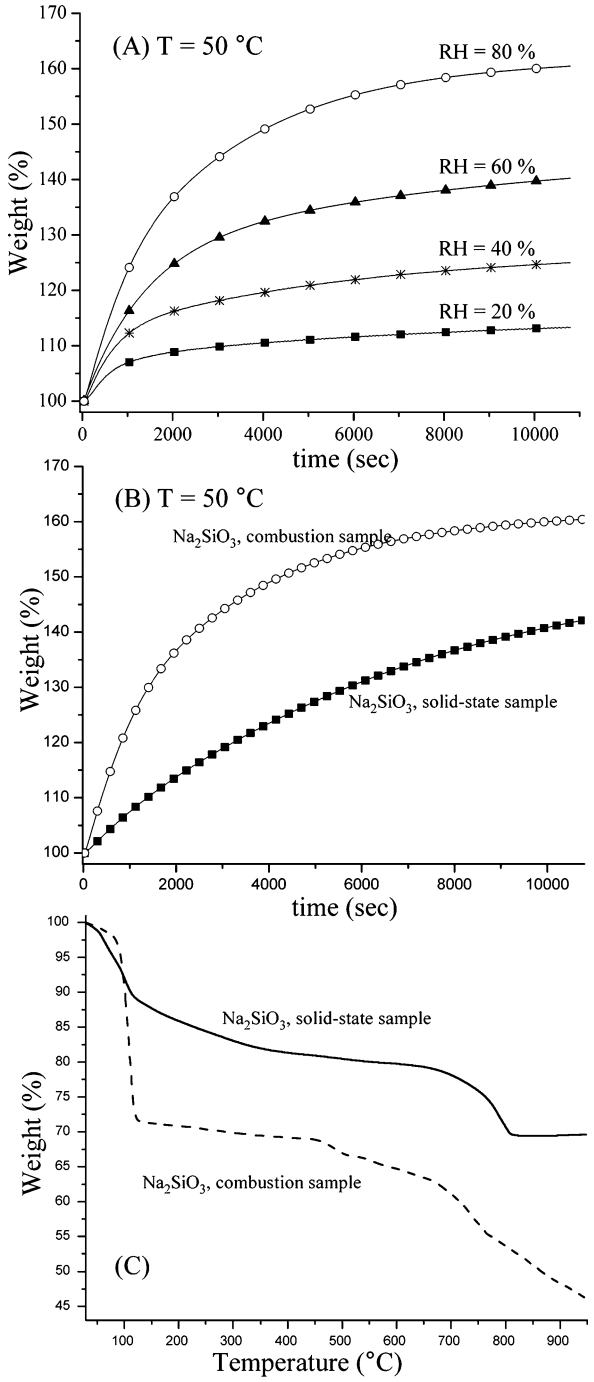


**Figure 14.** $Na_2SiO_3$ combustion isotherms treated at 50 °C at different RH. (A) Comparison of the $Na_2SiO_3$ solid-state and combustion isotherms performed at 50 °C and 80% of RH (B) and their corresponding decomposition TG (C). Each curve represents the experimental data, and the symbols were used to differentiate them.

samples were attributed to the different surface areas. Thus, $Na_2SiO_3$ must be considered as a possible option for the $CO_2$ capture process at moderated or environmental temperatures.

## AUTHOR INFORMATION


### Corresponding Author

*Phone +52 (55) 5622 4627, Fax +52 (55) 5616 1371, e-mail pfeiffer@iim.unam.mx (H.P.).


### Notes

The authors declare no competing financial interest.

## ACKNOWLEDGMENTS

This work was financially supported by the project SENER-CONACYT 150358. The authors thank A. Tejeda, O. Novelo, and M. A. Canseco for their technical help. Rafael Rodríguez-Mosqueda thanks CONACYT for financial support.

## REFERENCES


(1) Pires, J. C. M.; Martins, F. G.; Alvim-Ferraz, M. C. M.; Simões, M. Recent Developments on Carbon Capture and Storage: An Overview. *Chem. Eng. Res. Des.* **2011**, *89*, 1446−1460.

(2) Yang, D. A.; Chou, H. Y.; Kim, J.; Yang, S. T.; Ahn, W. S. $CO_2$ Capture and Conversion Using Mg-MOF-74 Preapred by a Sonochemical Method. *Energy Environ. Sci.* **2012**, *5*, 6465−6473.

(3) Zhao, Y.; Zhao, L.; Yao, K. X.; Yang, Y.; Zhang, Q.; Han, Y. Novel Porous Carbon Materials with Ultrahigh Nitrogen Contents for Selective $CO_2$ Capture. *J. Mater. Chem.* **2012**, *22*, 19726−19731.

(4) Zhai, Q. G.; Tao-Wu, Q. L.; Wang, L.; Zheng, S. T.; Bu, X.; Feng, P. High $CO_2$ and $H_2$ Uptake in an Anionic Porous Framework with Amino-Decorated Polyhedral Cages. *Chem. Mater.* **2012**, *24*, 2624−2626.

(5) Shen, W.; Zhang, S.; He, Y.; Li, J.; Fan, W. Hierarchical Porous Polyacrylonitrile-Based Activated Carbon Fibers for $CO_2$ Capture. *J. Mater. Chem.* **2011**, *21*, 14036−14040.

(6) Markewitz, P.; Kuckshinrichs, W.; Leitner, W.; Linssen, J.; Zapp, P.; Bongartz, R.; Schreiber, A.; Müller, T. E. Worldwide Innovations in the Development of Carbon Capture Technologies and the Utilization of $CO_2$. *Energy Environ. Sci.* **2012**, *5*, 7281−7305.

(7) Wang, M.; Lawal, A.; Stephenson, P.; Sidders, J.; Ramshaw, C. Post-combustion $CO_2$ Capture with Chemical Absorption: A State-of-the-Art Review. *Chem. Eng. Res. Des.* **2011**, *89*, 1609−1624.

(8) Pacciani, R.; Torres, J.; Solsona, P.; Coe, C.; Quinn, R.; Hufton, J.; Golden, T.; Vega, L. Influence of the Concentration of $CO_2$ and $SO_2$ on the Absorption of $CO_2$ by a Lithium Orthosilicate-Based Absorbent. F. *Environ. Sci. Technol.* **2011**, *45*, 7083−7088.

(9) Choi, S.; Dresse, J. H.; Jones, C. W. Adsorbent Materials for Carbon Dioxide Capture from Large Anthropogenic Point Sources. *ChemSusChem* **2009**, *2*, 796−854.

(10) D'Alessandro, D. M.; Smit, B.; Long, J. R. Carbon Dioxide Capture: Prospects for New Materials. *Angew. Chem., Int. Ed.* **2010**, *49*, 6058−6082.

(11) Nair, B. N.; Burwood, R. P.; Goh, V. J.; Nakagawa, K.; Yamaguchi, T. Lithium Based Ceramics Materials and membranes for High Temperature $CO_2$ Separation. *Prog. Mater. Sci.* **2009**, *54*, 511−541.

(12) Wang, Q.; Luo, J.; Zhong, Z.; Borgna, A. $CO_2$ Capture by Solid Adsorbents and their Applications; Current Status and New Trends. *Ener. Environ. Sci.* **2011**, *4*, 42−55.

(13) Hedin, N.; Chen, L. J.; Laaksonen, A. Sorbents for $CO_2$ Capture from Flue Gas-Aspects from Materials and Theoretical Chemistry. *Nanoscale* **2010**, *2*, 1819−1841.

(14) Pfeiffer, H. *Advances in $CO_2$ Conversion and Utilization*; ACS Symposium Series; Hu, Y. H., Ed.; American Chemical Society: Washington, DC, 2010; Vol. *1056*, pp 233−253.

(15) Duan, Y.; Luebke, D.; Pennline, H. Efficient Theoretical Screening of Solid Sorbents for $CO_2$ Capture Applications. *Int. J. Clean Coal Energy* **2012**, *1*, 1−11.

(16) Olivares-Marín, M.; Maroto-Valer, M. Development of Adsorbents for $CO_2$ Capture from Waste Materials: A Review. *Greenhouse Gases: Sci. Technol.* **2012**, *2*, 20−35.

(17) Korake, P. V.; Gaikwad, A. G. Capture of Carbon Dioxide Over Porous Solid Adsorbents Lithium Silicate, Lithium Aluminate and Magnesium Aluminate at Pre-Combustion Temperatures. *Front. Chem. Eng. China* **2011**, *5*, 215−226.

(18) Alcérreca-Corte, I.; Fregoso-Israel, E.; Pfeiffer, H. $CO_2$ Absorption on $Na_2ZrO_3$: A Kinetic Analysis of the Chemisorption and Diffusion Processes. *J. Phys. Chem. C* **2008**, *112*, 6520−6525.
(19) Santillán-Reyes, G. G.; Pfeiffer, H. Analysis of the $CO_2$ Capture in Sodium Zirconate ($Na_2ZrO_3$). Effect of the Water Vapor Addition. *Int. J. Greenhouse Gas Control* **2011**, *5*, 1624−1629.
(20) Halabi, M. H.; de Croon, J.; van der Schaaf, J.; Cobden, P. D.; Schouten, J. C. Reactor Modeling of Sorption-Enhanced Autothermal Reforming of Methane. Part I: Performance Study of Hydrotalcite and Lithium Zirconate-Based Processes. *Chem. Eng. J.* **2011**, *168*, 872−882.
(21) Xiao, Q.; Tang, X.; Liu, Y.; Zhong, Y.; Zhu, W. Citrate Route to Prepare K-Doped $Li_2ZrO_3$ Sorbents with Excellent $CO_2$ Capture Properties. *Chem. Eng. J.* **2011**, *174*, 231−235.
(22) Iwan, A.; Stephenson, H.; Ketchie, W. C.; Lapkin, A. A. High Temperature Sequestration of $CO_2$ Using Lithium Zirconates. *Chem. Eng. J.* **2009**, *146*, 249−258.
(23) Yin, X. S.; Zhang, Q. H.; Yu, J. G. Three-Step Calcination Synthesis of High-Purity $Li_8ZrO_6$ with $CO_2$ Absorption Properties. *Inorg. Chem.* **2011**, *50*, 2844−2850.
(24) Yin, X. S.; Song, M.; Zhang, Q. H.; Yu, J. G. High-Temperature $CO_2$ Capture on $Li_6Zr_2O_7$: Experimental and Modeling Studies. *Ind. Eng. Chem. Res.* **2010**, *49*, 6593−6598.
(25) Radfarnia, H. R.; Iliuta, M. C. Surfactant-Template/Ultrasound-Assisted Method for the Preparation of Porous Nanoparticle Lithium Zirconate. *Ind. Eng. Chem. Res.* **2011**, *50*, 9295−9305.
(26) Yin, X. S.; Li, S. P.; Zhang, Q. H.; Yu, J. G. Synthesis and $CO_2$ Adsorption Characteristics of Lithium Zirconates with High Lithia Content. *J. Am. Ceram. Soc.* **2010**, *93*, 2837−2842.
(27) Xiao, Q.; Liu, Y.; Zhong, Y.; Zhu, W. A Citrate Sol-Gel Method to Synthesize $Li_2ZrO_3$ Nanocrystals with Improved $CO_2$ Capture Properties. *J. Mater. Chem.* **2011**, *21*, 3838−3842.
(28) Khokhani, M.; Khomane, R. B.; Kulkarni, B. D. Sodium-Doped Lithium Zirconate Nano Squares: Synthesis, Characterization and Applications for $CO_2$ Sequestration. *J. Sol-Gel Sci. Technol.* **2012**, *61*, 316−320.
(29) Kang, S. Z.; Wu, T.; Li, X.; Mu, J. Low Temperature Biomimetic Synthesis of the $Li_2ZrO_3$ Nanoparticles Containing $Li_6Zr_2O_7$ and High Temperature $CO_2$ Capture. *Mater. Lett.* **2010**, *64*, 1404−1406.
(30) Martínez-dlCruz, L.; Pfeiffer, H. Towards Understanding the Effect of Water Sorption on Lithium Zirconate ($Li_2ZrO_3$) During its Carbonation Process at Low Temperatures. *J. Phys. Chem. C* **2010**, *114*, 9453−9458.
(31) Shan, S.; Jia, Q.; Jiang, L.; Wang, Y. Effect of different Silicon Sources on $CO_2$ Absorption Properties of $Li_4SiO_4$ at High Temperatures. *Adv. Mater. Res.* **2011**, *213*, 515−518.
(32) Olivares-Marín, M.; Drage, T. C.; Maroto-Valer, M. Novel Lithium-Based Sorbents from Fly Ashes for $CO_2$ Capture at High Temperatures. *Int. J. Greenhouse Gas Control* **2010**, *4*, 623−629.
(33) Duan, Y. Structural and Electronic properties of $Li_8ZrO_6$ and Its $CO_2$ Capture Capabilities: An *ab initio* Thermodynamic Approach. *Phys. Chem. Chem. Phys.* **2013**, *15*, 9752−9760.
(34) Inoue, R.; Ueda, S.; Wakuta, K.; Sasaki, K.; Ariyama, T. Thermodinamic Consideration on the Absorption Properties of Carbon Dioxide to Basic Oxide. *ISIJ Int.* **2010**, *50*, 1532−1538.
(35) Wang, K.; Guo, X.; Zhao, P.; Wang, F.; Zheng, C. High Temperature Capture of $CO_2$ on Lithium-Based Sorbents from Rise Husk Ash. *J. Hazard. Mater.* **2011**, *189*, 301−307.
(36) Duan, Y.; Parlinski, K. Density Function Theory Study on the Structural, Electronic, Lattice Dynamical, and Thermodynamic Properties of $Li_4SiO_4$ and Its Capability for $CO_2$ Capture. *Phys. Rev. B* **2011**, *84*, 104113.
(37) Ávalos-Rendón, T.; Casa-Madrid, J.; Pfeiffer, H. Thermochemical Capture of Carbon Dioxide on Lithium Aluminates ($LiAlO_2$ and $Li_5AlO_4$): A New Option for the $CO_2$ Absorption. *J. Phys. Chem. A* **2009**, *113*, 6919−6923.
(38) Ueda, S.; Inoue, R.; Sasaki, K.; Wakuta, K.; Ariyama, T. $CO_2$ Absorption and Desorption Abilities of $Li_2O$-$TiO_2$ Compounds. *ISIJ Int.* **2011**, *51*, 530−537.
(39) Ortiz-Landeros, J.; Ávalos-Rendón, T.; Gómez-Yáñez, C.; Pfeiffer, H. Analysis and Perspectives Concerning $CO_2$ Chemisorption on Lithium Ceramics Using Thermal Analysis. *J. Therm. Anal. Calorim.* **2012**, *108*, 647−655.
(40) Rodríguez-Mosqueda, R.; Pfeiffer, H. Thermokinetic Analysis of the $CO_2$ Chemisorption on $Li_4SiO_4$ by Using Different Gas Flow Rates and Particle Sizes. *J. Phys. Chem. A* **2010**, *114*, 4535−4541.
(41) Qi, Z.; Daying, H.; Yang, L.; Qian, Y.; Zibin, Z. Analysis of $CO_2$ Sorption/Desorption Kinetic Behaviors and Reaction Mechanism on $Li_4SiO_4$. *AIChE J.* **2013**, *59*, 901−911.
(42) Quinn, R.; Kitzhoffer, R. J.; Hufton, J. R.; Golden, T. C. A High Temperature Lithium Orthosilicate-Based Solid Absorbent for Post Combustion $CO_2$ Capture. *Ind. Eng. Chem. Res.* **2012**, *51*, 9320−9327.
(43) Xiao, Q.; Tang, X.; Zhong, Y.; Zhu, W. A Facile Starch-Assisted Sol-Gel Method to Synthesize K-Doped $Li_2ZrO_3$ Sorbents with Excellent $CO_2$ Capture Properties. *J. Am. Ceram. Soc.* **2012**, *95*, 1544−1548.
(44) Radfarnia, H. R.; Iliuta, C. R. Application of Surfactant-Template Technique for Preparation of Sodium Zirconate as High Temperature $CO_2$ Sorbent. *Separ. Purif. Technol.* **2012**, *93*, 98−106.
(45) Khomane, R. B.; Sharma, B. K.; Saha, S.; Kulkarni, B. D. Reverse Microemulsion Mediated Sol-Gel Synthesis of Lithium Silicate Nanoparticles Under Ambient Conditions: Scope for $CO_2$ Sequestration. *Chem. Eng. Sci.* **2006**, *61*, 3415−3418.
(46) Ortiz-Landeros, J.; Gómez-Yáñez, C.; Pfeiffer, H. Surfactant-Assisted Hydrothermal Crystallization of Nanostructured Lithium Metasilicate ($Li_2SiO_3$) Hollow Spheres: II. Textural Analysis and $CO_2$-$H_2O$ Sorption Evaluation. *J. Solid State Chem.* **2011**, *184*, 2257−2262.
(47) Rodríguez, M. T.; Pfeiffer, H. Sodium Metasilicate ($Na_2SiO_3$): A Thermokinetic Analysis of Its $CO_2$ Chemical Sorption. *Thermochim. Acta* **2008**, *473*, 92−95.
(48) Lowell, S.; Shields, J. E.; Thomas, M. A. *Characterization of Porous Solids and Powders: Surface Area, Pore Size and Density*; Particle Technology Series; Kluwer Academic Publishers: London, 2004.
(49) Ávalos-Rendón, T. L.; Pfeiffer, H. High $CO_2$ Chemisorption in $\alpha$-$Li_5AlO_4$ at Low Temperatures (30−80 °C): Effect of the Water Vapor Addition. *Energy Fuels* **2012**, *26*, 3110−3114.
(50) Nakamoto, K. *Infrared and Raman Spectra of Inorganic and Coordination Compounds*; Wiley: New York, 2004.
(51) Huang, C. K.; Paul, F. Infrared Study of the Carbonate Minerals. *Am. Mineral.* **1960**, *45*, 311−325.
(52) Dei, L.; Guarini, G. G. T. The Thermal Decomposition of $NaHCO_3$. *J. Therm. Anal. Calorim.* **1997**, *50*, 773−783.
(53) Heda, P. K.; Dollimore, D.; Alexander, K. S.; Chen, D.; Law, E.; Bicknell, P. A Method of Assessing Solid State Reactivity Illustrated by Thermal Decomposition Experiments on Sodium Bicarbonate. *Thermochim. Acta* **1995**, *255*, 255−272.